eLIFE
elifesciences.org

RESEARCH ARTICLE

Figures and figure supplements

Gradient-reading and mechano-effector machinery for netrin-1-induced axon guidance

Kentarou Baba *et al*

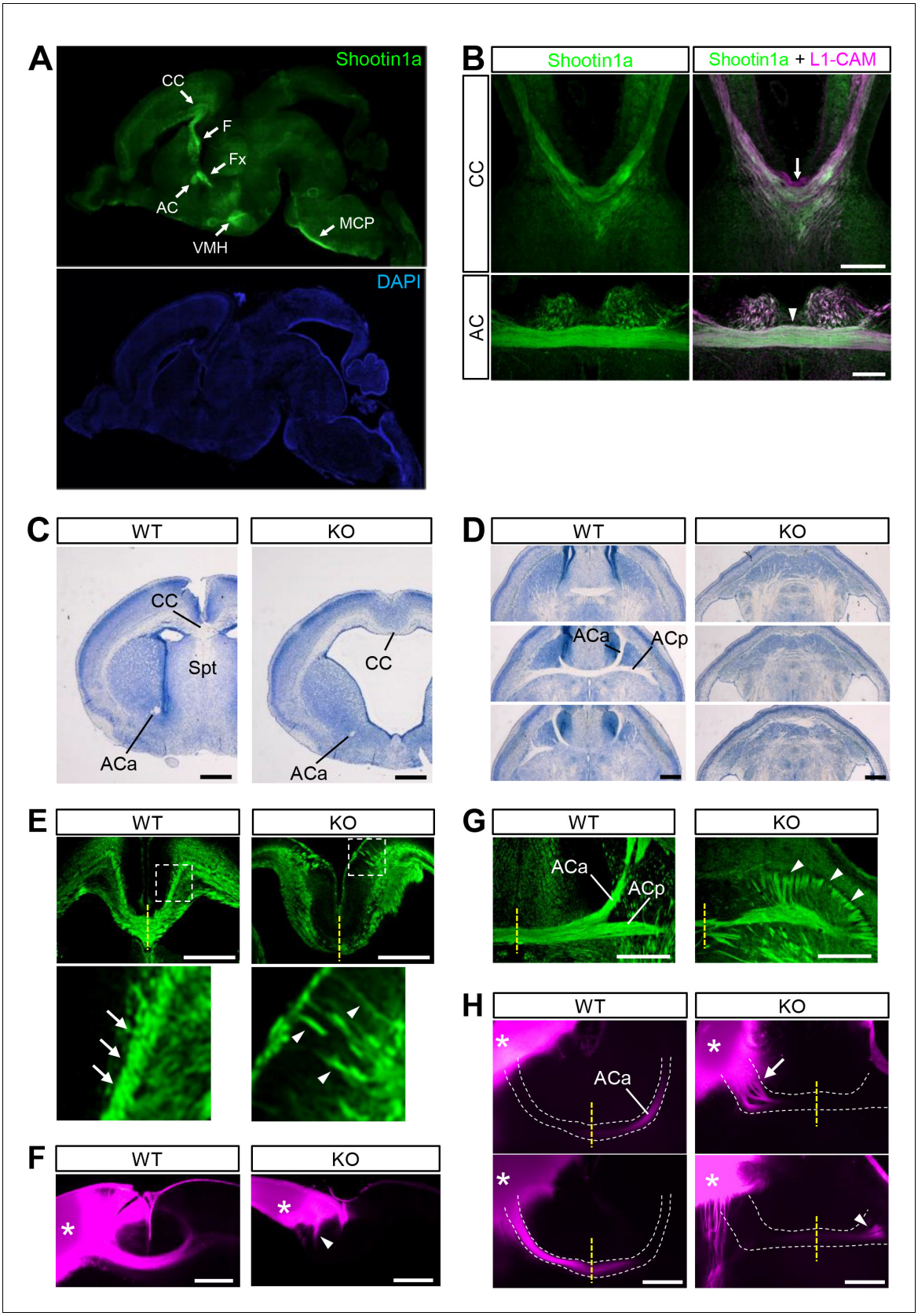

Figure 1. *Shootin1* knockout mice display abnormal projection of forebrain commissural axons. (**A**) A representative sagittal section of a P0 mouse brain immunolabeled with shootin1a antibody (green) and counterstained with DAPI (blue). (**B**) Coronal sections of E16.5 mouse brains double-

Figure 1 continued on next page

Figure 1 continued

immunolabeled with anti-shootin1a (green) and anti-L1-CAM (magenta) antibodies. The arrow and arrowhead indicate the corpus callosum and anterior commissure, respectively. (**C**) Coronal sections of the forebrain of wild-type and *Shootin1* knockout mice at P0 stained for Nissl substance. (**D**) Serial horizontal sections of the ventral forebrain of wild-type and *Shootin1* knockout mice at P0 stained for Nissl substance. (**E**) Coronal sections of wild-type and *Shootin1* knockout mouse brains at P0 immunolabeled with anti-L1-CAM antibody (green). Ectopic axonal projections were observed in the neocortex (arrowheads). In the knockout mice, the prominent axonal tracts observed in the intermediate zone of the neocortex of wild-type mice (arrows) were undetectable and ectopic axonal projections were observed (arrowheads). Lower panels show enlarged views of the rectangles. (**F**) Coronal sections of wild-type and *Shootin1* knockout mouse brains at P0. DiI crystals (magenta) were placed into the neocortex (asterisks) to label callosal axons. An arrowhead indicates incomplete contralateral projections of callosal axons. (**G**) Horizontal sections of wild-type and *Shootin1* knockout mouse brains at P0 immunolabeled with anti-L1-CAM antibody (green). In *Shootin1* knockout mice, the bundling of the commissural axons was disrupted (arrowheads). (**H**) Horizontal sections of wild-type and *Shootin1* knockout mouse brains at P0. DiI crystals (magenta) were placed in the anterior piriform cortex (asterisks) to label the anterior limb of the anterior commissure. Defasciculation and misprojection of the commissural axons are indicated by the arrow and arrowhead, respectively. Dashed lines indicate the anterior limb of the anterior commissure. Abbreviations: AC, anterior commissure; ACa, anterior limb of the anterior commissure; ACp, posterior limb of the anterior commissure; CC, corpus callosum; F, fimbria; Fx, fornix; KO, *Shootin1* knockout mouse; MCP, middle cerebellar peduncle; Spt, Septum; VMH, ventromedial hypothalamic nucleus; WT, wild-type mouse. Scale bars: 500 μm.

DOI: https://doi.org/10.7554/eLife.34593.003

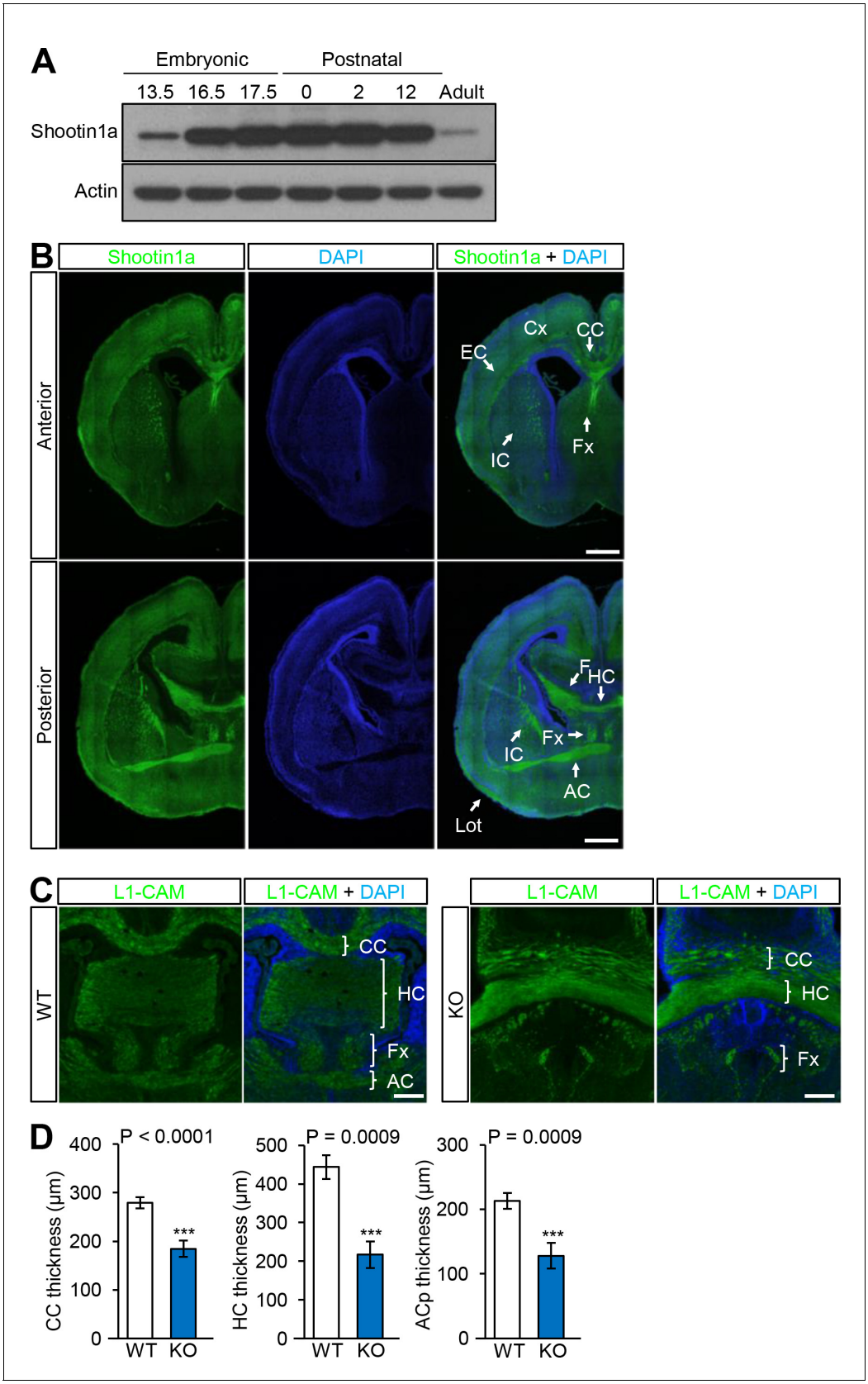

Figure 1—figure supplement 1. Expression and distribution of shootin1a in mouse brain and phenotype of *Shootin1* knockout mice forebrain. (**A**) Immunoblot analysis of shootin1a in mouse brain at various developmental stages. The same amounts (20 μg) of protein were loaded in each lane and

Figure 1—figure supplement 1 continued on next page

Figure 1—figure supplement 1 continued

immunoblotted by anti-shootin1a and anti-actin antibodies. (**B**) Coronal sections of P0 mouse brains immunolabeled with shootin1a antibody (green) and counter-stained with DAPI (blue). Bars: 500 μm. (**C**) Coronal sections of P0 brain from wild-type and *Shootin1* knockout mouse at P0 labeled with anti-L1-CAM (green) antibody and DAPI (blue). Bars: 200 μm. (**D**) Quantitative analyses of the thickness of the corpus callosum (WT, $n = 9$; KO, $n = 18$), hippocampal commissure (WT, $n = 5$; KO, $n = 6$) and anterior commissure (WT, $n = 9$; KO, $n = 18$). The thicknesses were measured at the midline of the commissures of Nissl-stained sections. Data represent means ± SEM; ***$p<0.01$ (unpaired Student's *t*-test). Abbreviations: Cx, cerebral cortex; EC, external capsule; HC, hippocampal commissure; IC, internal capsule; Lot, lateral olfactory tract.

DOI: https://doi.org/10.7554/eLife.34593.004

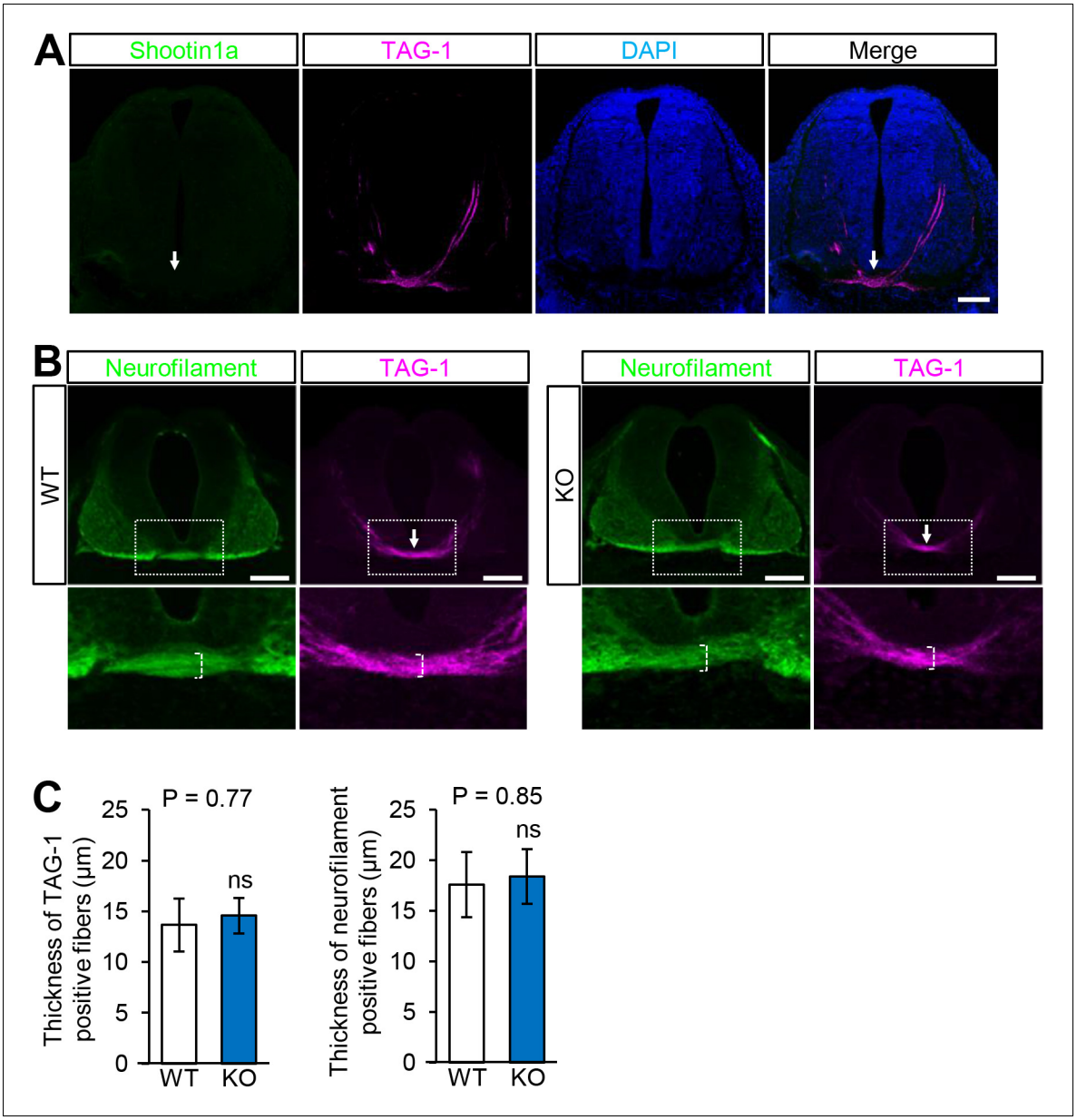

Figure 1—figure supplement 2. Distribution of shootin1a in mouse spinal cord and phenotype of *Shootin1* knockout spinal cord. (**A**) A coronal section of E12.5 mouse spinal cord labeled with anti-shootin1a antibody (green), anti-TAG-1 (magenta) antibody and DAPI (blue). TAG-1 is a marker for ventral spinal commissural axons (***Dodd et al., 1988***). The arrows indicate the ventral commissure. Bar: 500 μm. (**B**) Coronal sections of the spinal cord at E12.5 from wild-type and *Shootin1* knockout mice labeled with aniti-neurofilament (green) and anti-TAG-1 (magenta) antibodies. The arrows indicate the ventral commissure. The images below show enlarged views of the ventral commissures in the rectangles. Bars: 500 μm. (**C**) Quantitative analyses of the thickness of the ventral spinal commissure of wild-type and *Shootin1* knockout mice labeled with anti-neurofilament and anti-TAG-1 antibodies in (**B**). The thicknesses were measured at the midline of the commissures (B, dashed square brackets) (WT, $n = 9$; KO, $n = 9$). Data represent means ± SEM; ns, not significant (unpaired Student's *t*-test).

DOI: https://doi.org/10.7554/eLife.34593.006

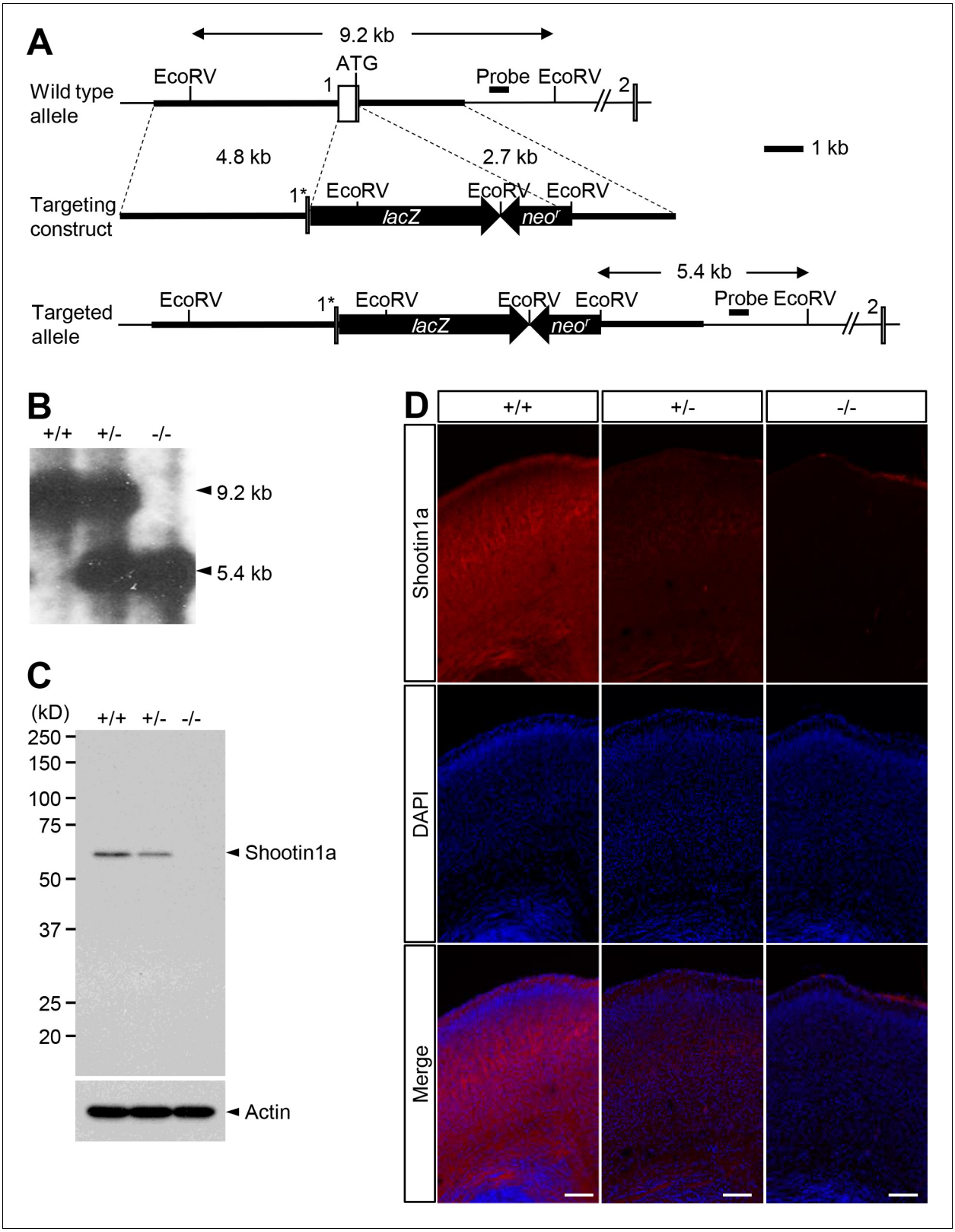

Figure 1—figure supplement 3. Generation of *Shootin1* knockout mice. (**A**) Schematic representations of *Shootin1* gene-targeting strategy. Upper panel, *Shootin1* genomic locus including exons 1 and 2. Middle panel, targeting vector for homologous recombination. The targeting vector deleted a 509-base genomic sequence including exon one with the start codon (asterisk). Lower panel, targeted gene after homologous recombination. The

Figure 1—figure supplement 3 continued on next page

Figure 1—figure supplement 3 continued

probe used in Southern blot analysis is indicated. (**B**) Genomic DNAs isolated from wild-type (+/+), heterozygous (+/-) and homozygous (-/-) mouse tails were digested with EcoRV and then analyzed by Southern blot analysis using the probe. DNA fragments of 9.2 and 5.4 kb are expected for the wild-type allele and mutant allele, respectively. (**C**) Immunoblot analysis of brain lysates prepared from wild-type (+/+), heterozygous (+/-) and homozygous (-/-) mouse brains, at P0 using anti-shootin1a and anti-actin antibodies. (**D**) Coronal sections of mouse cerebral cortex at P0 from wild-type (+/+), heterozygous (+/-) and homozygous (-/-) mice labeled with anti-shootin1a antibody (red) and DAPI (blue). Bars: 500 μm.

DOI: https://doi.org/10.7554/eLife.34593.008

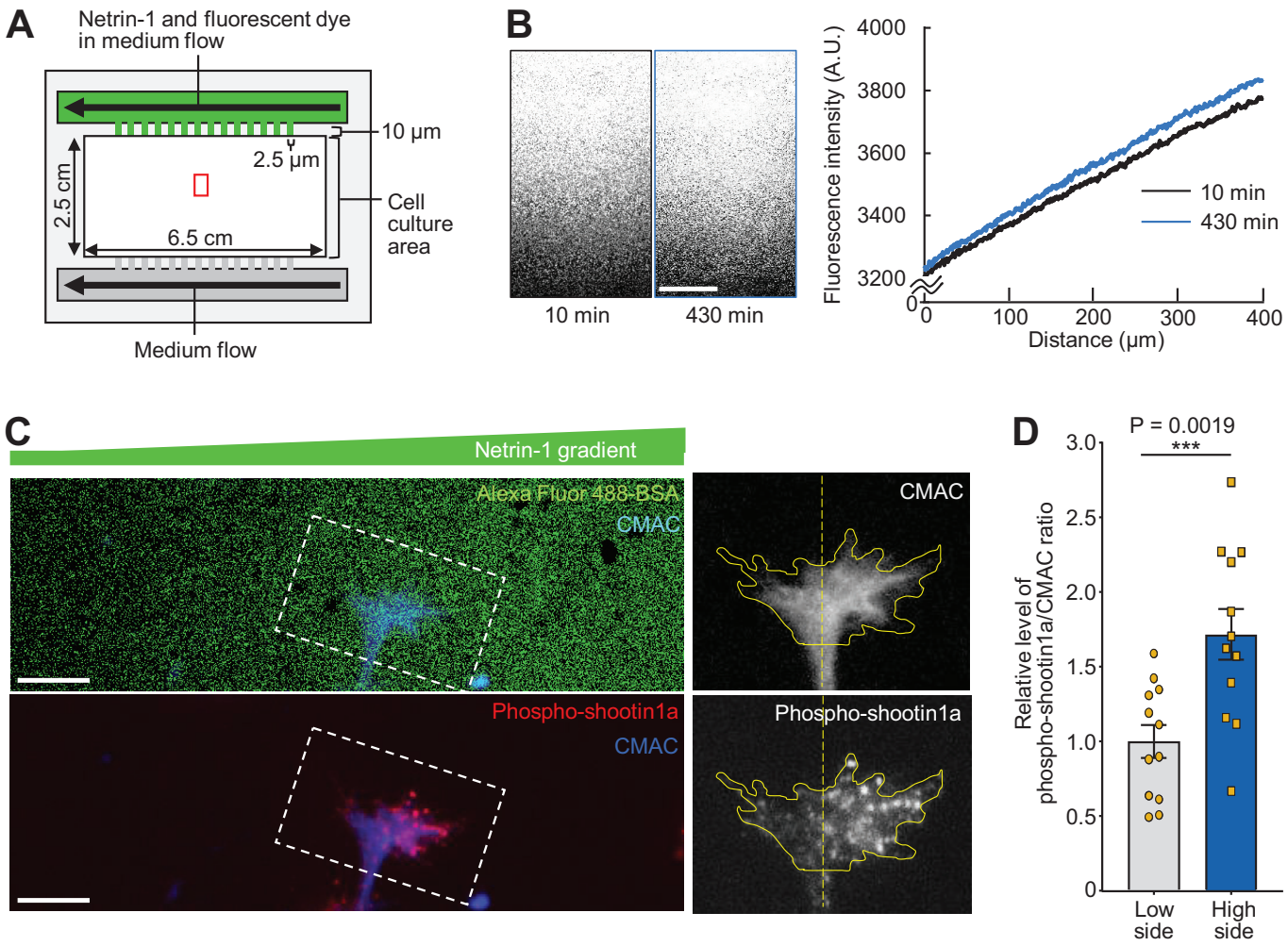

Figure 2. Netrin-1 gradients induce asymmetrically localized phosphorylation of shootin1a within single growth cones. (**A**) A schematic diagram of the device with microjet arrays that generates gradients of diffusible molecules in the culture medium. (**B**) Time-lapse fluorescence images of fluorescent dye (Alexa Fluor 488-BSA) in the cell culture area of the device in (A, red rectangle). See ***Video 1***. The graph (right) depicts line scans of the fluorescence intensity across the field at 10 min (black line) and 430 min (blue line) during time-lapse imaging. A stable gradient of Alexa Fluor 488-BSA was generated in the device. Bar: 100 µm. (**C**) Neurons cultured in the device were labeled with CMAC (blue) and exposed to gradients of netrin-1 and Alexa Fluor 488-BSA (green) for 30 min. They were then fixed and immunolabeled with an antibody that recognizes shootin1a phosphorylation at Ser249 (red). The right panels show the fluorescent signals of CMAC and phospho-shootin1a in the growth cone located in the corresponding dashed rectangle. Yellow lines and dotted lines indicate the boundary and center line of the growth cone, respectively. A higher level of phospho-shootin1a immunolabeling was observed on the netrin-1 source side. Bar: 10 µm. (**D**) Quantification of relative phospho-shootin1a immunolabeling levels (phosopho-shootin1a immunoreactivity/CMAC staining) in the netrin-1 source side (high side) and control side (low side) of single growth cones. $n = 12$ growth cones. Data represent means ± SEM; ***$p<0.01$ (unpaired Student's *t*-test).

DOI: https://doi.org/10.7554/eLife.34593.009

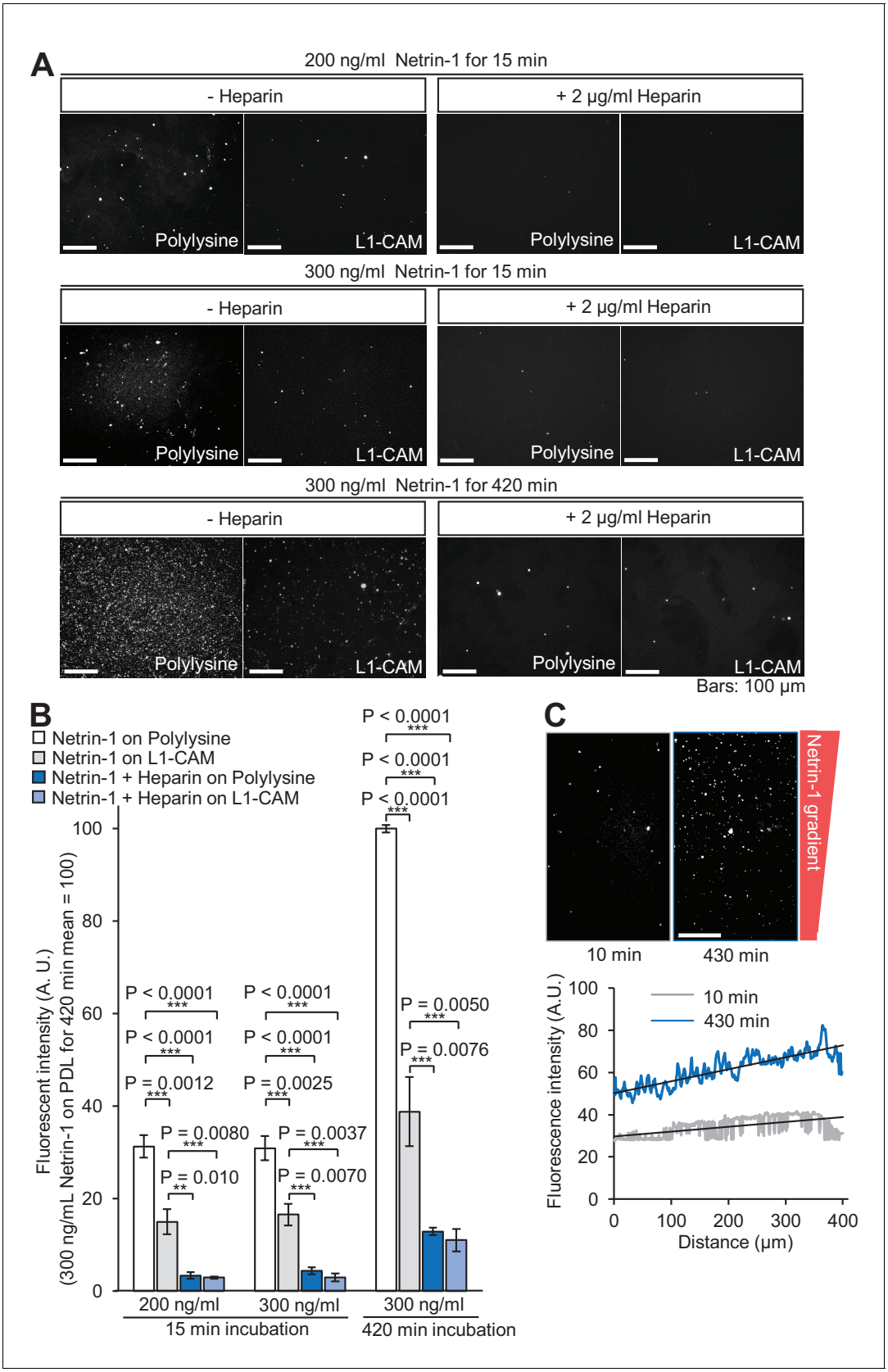

Figure 2—figure supplement 1. Netrin-1 gradients produced on the substrate. (**A**) Glass coverslips coated with polylysine or coated sequentially with polylysine and L1-CAM-Fc were incubated with the culture medium and netrin-1 containing a 10-His tag at the C-terminus, in the absence or presence

Figure 2—figure supplement 1 continued on next page

Figure 2—figure supplement 1 continued

of 2 μg/ml heparin. The glasses were then labeled with anti-His antibody and fluorescence images were acquired using a fluorescence microscope. (**B**) Quantitative analyses of the netrin-1 attached to the glass coverslips in (**A**). Fluorescence images were acquired using a fluorescence microscope and quantified using ImageJ. Data represent means ± SEM (n = 3 independent experiments); ***p<0.01; **p<0.02 (one-way ANOVA with Tukey's post hoc test). (**C**) Glass coverslips coated sequentially with polylysine and L1-CAM-Fc were incubated for 10 or 430 min with the netrin-1 gradients produced by the device in ***Figure 2A*** (red rectangle). The glasses were then labeled with anti-His antibody, and fluorescence images of netrin-1 were acquired using a fluorescence microscope. The lower graph depicts line scans of the immunolabeled netrin-1 across the field (upper panels). The black lines were fitted with a least-squares method. The differences in the netrin-1 concentrations at the source side end and the other end of the area that expands 400 μm of the linear gradient, estimated by the fluorescence intensity, were 24% for 10 min and 31% for 430 min, respectively. As the regular growth cone width of cultured hippocampal neurons is about 10 μm, we estimate that the gradient steepness of netrin-1 that covers growth cones is about 0.6% at 10 min and 0.8% at 430 min. Bars: 100 μm.

DOI: https://doi.org/10.7554/eLife.34593.010

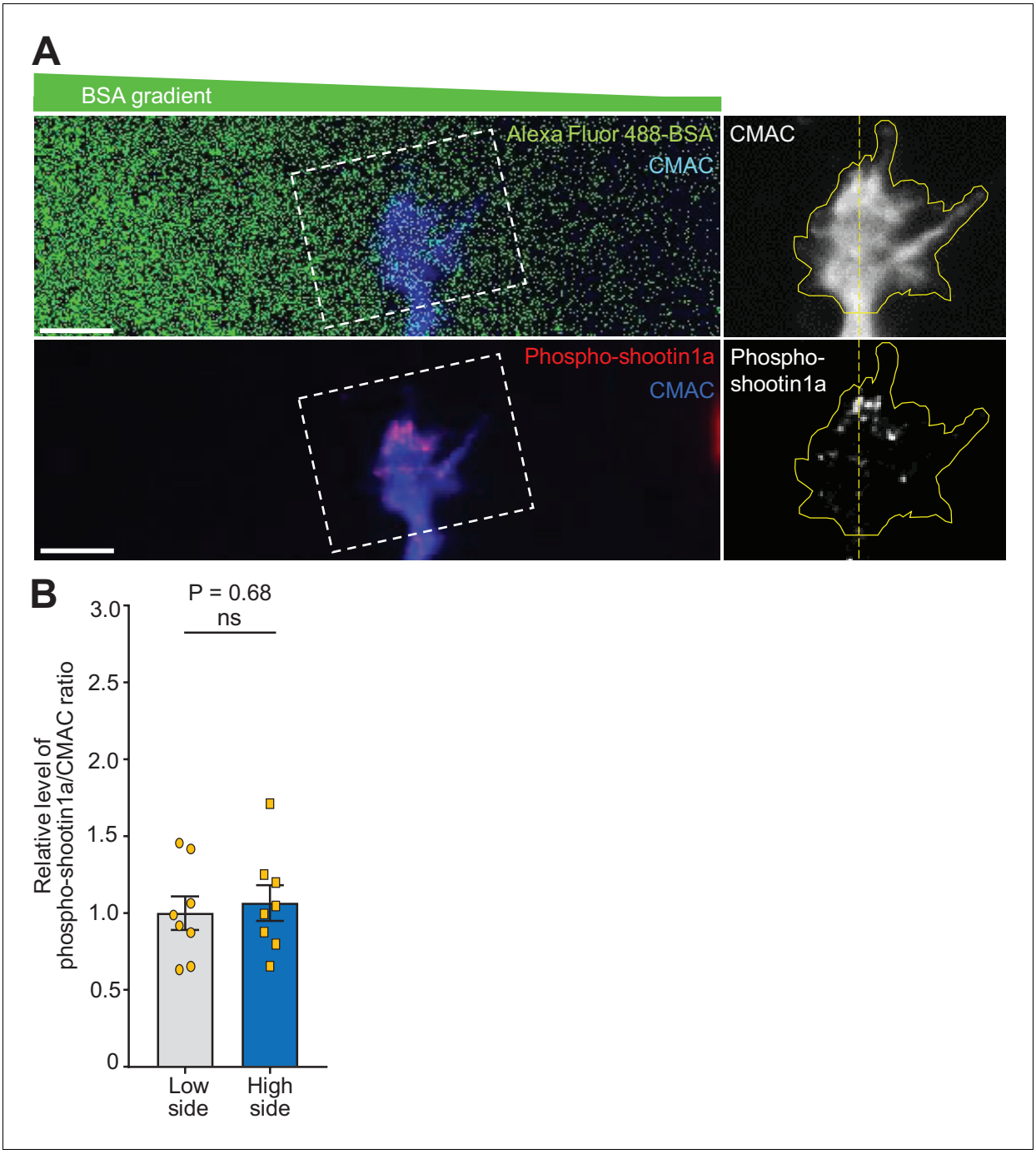

Figure 2—figure supplement 2. BSA gradients do not elicit polarized phosphorylation of shootin1 within growth cones. (**A**) Neurons cultured in the device (***Figure 2A***, red rectangle) were labeled with CMAC (blue) and exposed to gradients of Alexa Fluor 488-BSA (green) for 30 min. They were then fixed and immunolabeled with an antibody that recognizes shootin1a phosphorylation at Ser249 (red). The right panels show the fluorescence signals of CMAC and phospho-shootin1a in the growth cone located in the corresponding dashed rectangle. Yellow lines and dotted lines indicate the boundary and center line of the growth cone, respectively. Bar: 10 μm. (**B**) Quantification of relative phospho-shootin1a immunolabeling levels (phosopho-shootin1a immunoreactivity/CMAC staining) in the BSA source side (high side) and control side (low side) of single growth cones. n = 8 growth cones. Data represent means ± SEM; ns, not significant (unpaired Student's t-test).

DOI: https://doi.org/10.7554/eLife.34593.012

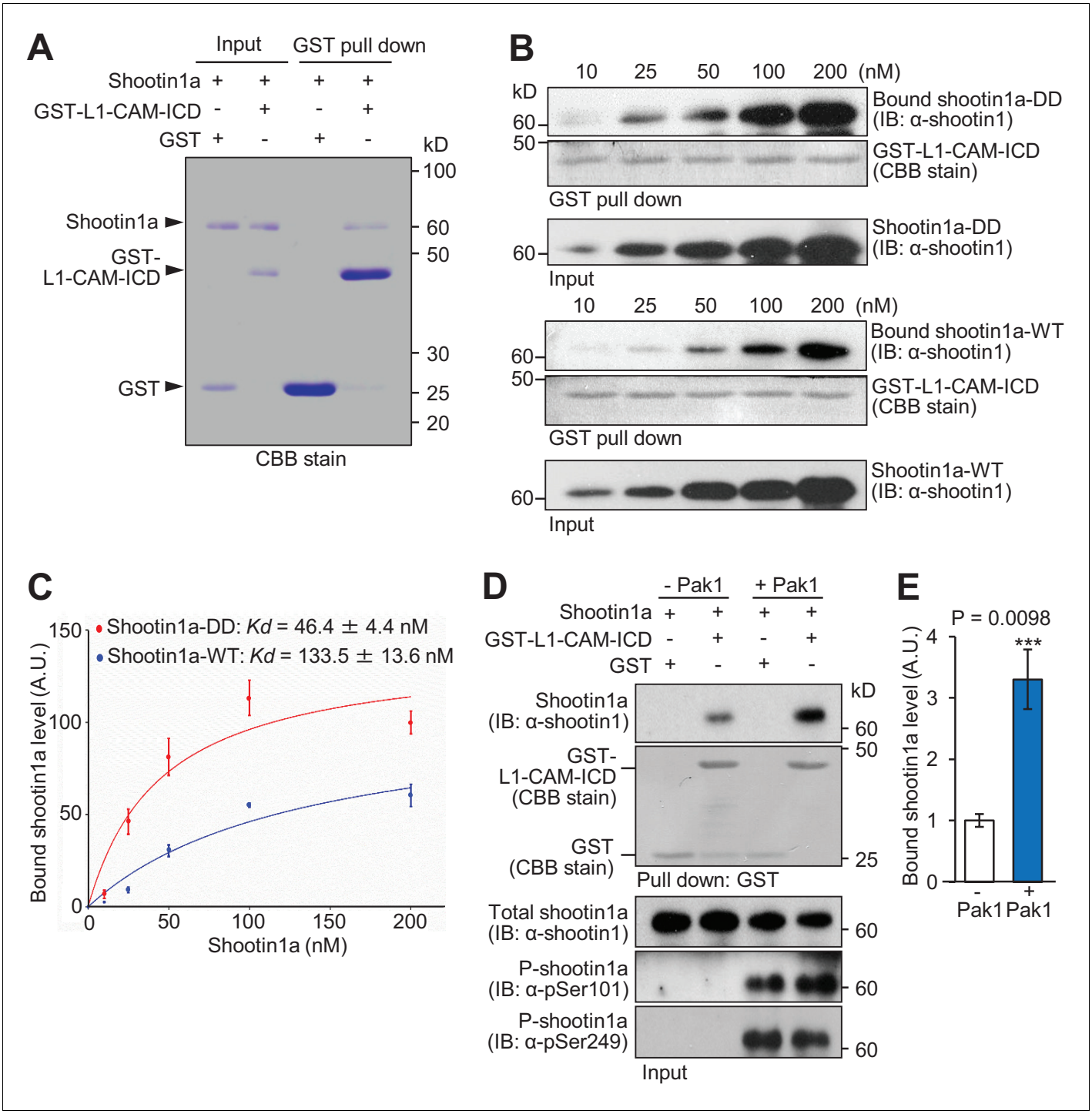

Figure 3. Pak1-mediated shootin1a phosphorylation enhances the interaction between shootin1a and L1-CAM. (**A**) In vitro binding assay using purified shootin1a-WT (100 nM) and purified GST-L1-CAM-ICD (100 nM). Proteins were incubated with Glutathione Sepharose 4B and GST-L1-CAM-ICD was eluted. The eluate was then analyzed by SDS-PAGE and CBB staining; 0.2% of the input proteins were also analyzed. (**B** and **C**) In vitro binding assay using purified shootin1a-WT or purified shootin1a-DD and purified GST-L1-CAM-ICD. Shootin1a-DD or shootin1a-WT at increasing concentrations was incubated with GST-L1-CAM-ICD and Glutathione Sepharose 4B. GST-L1-CAM-ICD was eluted. After SDS-PAGE, the eluate was immunoblotted with anti-shootin1 antibody or stained with CBB (**B**), and the bound shootin1a-DD and shootin1a-WT were then quantified (**C**). Data represent means ± SEM (n = 3 independent experiments). (**D** and **E**) In vitro binding assay using Pak1-phosphorylated purified shootin1a and purified GST-L1-CAM-ICD. Shootin1a-WT (100 nM) or Pak1-phosphorylated shootin1a-WT (100 nM) was incubated with GST-L1-CAM-ICD and Glutathione Sepharose 4B. GST-L1-CAM-ICD was eluted. After SDS-PAGE, the eluate was immunoblotted with anti-shootin1 antibody or stained with CBB (**D**). Input proteins (1%) were

Figure 3 continued on next page

Figure 3 continued

also analyzed with anti-shootin1, anti-pSer101-shootin1 or anti-pSer249-shootin1 antibody. Quantitative data for bound shootin1a are shown in (**E**) (n = 3 independent experiments). Data represent means ± SEM; ***p<0.01 (unpaired Student's t-test).

DOI: https://doi.org/10.7554/eLife.34593.016

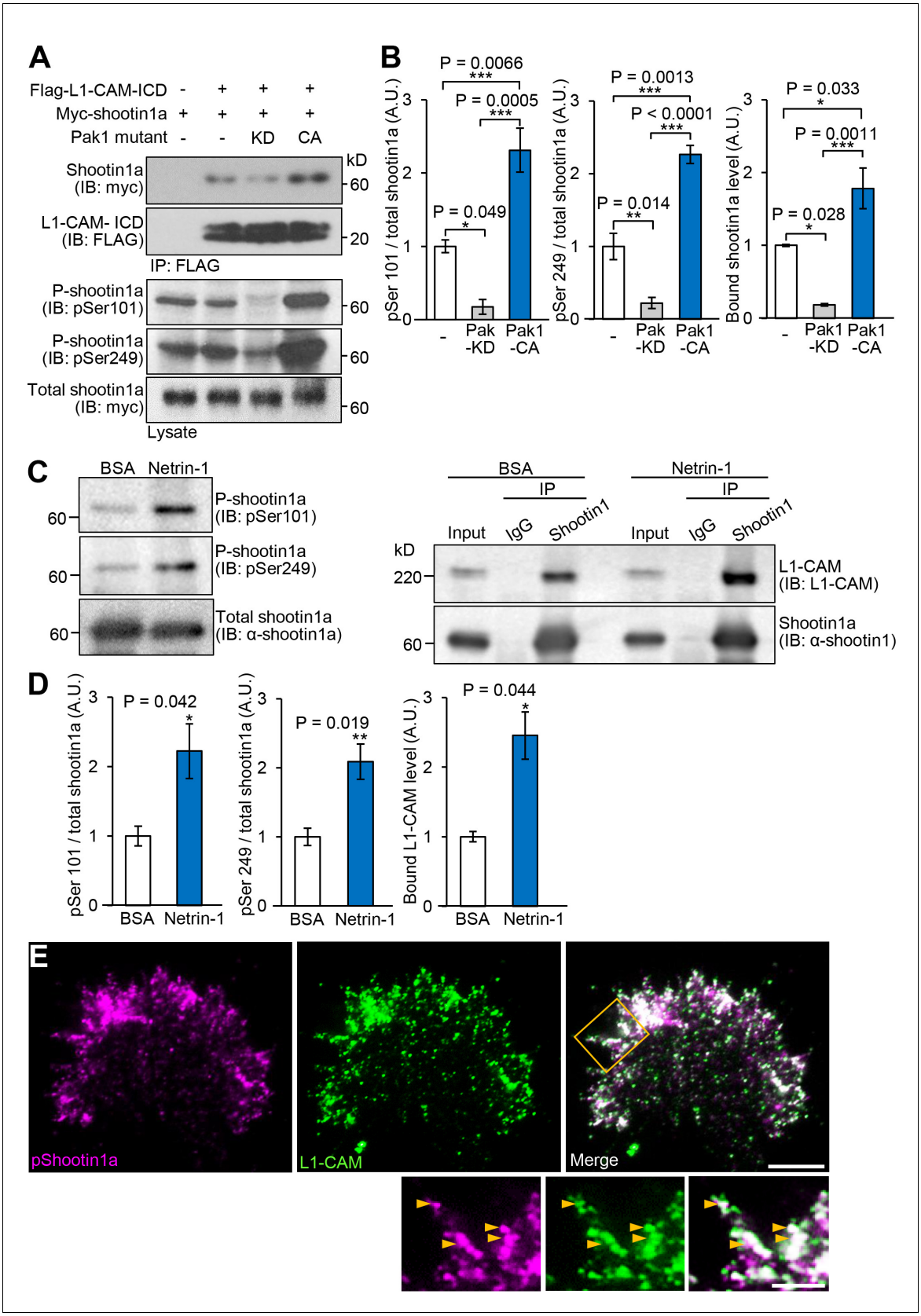

Figure 4. Netrin-1–induced Pak1-mediated shootin1a phosphorylation enhances the interaction between shootin1a and L1-CAM. (**A** and **B**) Co-immunoprecipitation of myc-shootin1a and FLAG-L1-CAM-ICD in HEK293T cells. Cells were transfected with vectors to express myc-shootin1a and

Figure 4 continued on next page

Figure 4 continued

FLAG-L1-CAM-ICD; some of them were also co-transfected with a vector to express dominant negative Pak1 (KD) or constitutively active Pak1 (CA) as indicated. Cell lysates were then incubated with anti-FLAG antibody. The immunoprecipitates were immunoblotted with anti-myc or anti-FLAG antibody (**A**). Cell lysates (1%) were also analyzed with anti-pSer101-shootin1, anti-pSer249-shootin1, or anti-myc antibody. Quantitative data for phosphorylated and bound shootin1a are shown in (**B**) (n = 3 independent experiments). Data represent means ± SEM; ***p<0.01; **p<0.02; *p<0.05 (One-way ANOVA with Tukey's post hoc test). (**C** and **D**) Co-immunoprecipitation of shootin1a and L1-CAM in cultured cortical neurons. After incubation of neurons with 4.4 nM netrin-1 or BSA (control) for 1 hr, cell lysates were prepared and incubated with anti-shootin1 antibody (right panel). The immunoprecipitates were immunoblotted with anti-shootin1 or anti-L1-CAM antibody. The cell lysates (5%) were also analyzed with anti-pSer101-shootin1, anti-pSer249-shootin1, or anti-shootin1a antibody (left panel). Quantitative data for phosphorylated shootin1a and bound L1-CAM are shown in (**D**) (n = 3 independent experiments). Data represent means ± SEM; **p<0.02; *p<0.05 (Unpaired Student's t-test). (**E**) Fluorescence images of an axonal growth cone labeled with anti-pSer249-shootin1a (magenta) and anti-L1-CAM (green) antibodies. The cells were observed using a TIRF microscope. An enlarged view of the filopodium in the rectangle is shown in the lower panel. Arrowheads indicate phosphorylated shootin1a colocalized with L1-CAM. Bar: 5 μm (in the inset, 2 μm).

DOI: https://doi.org/10.7554/eLife.34593.019

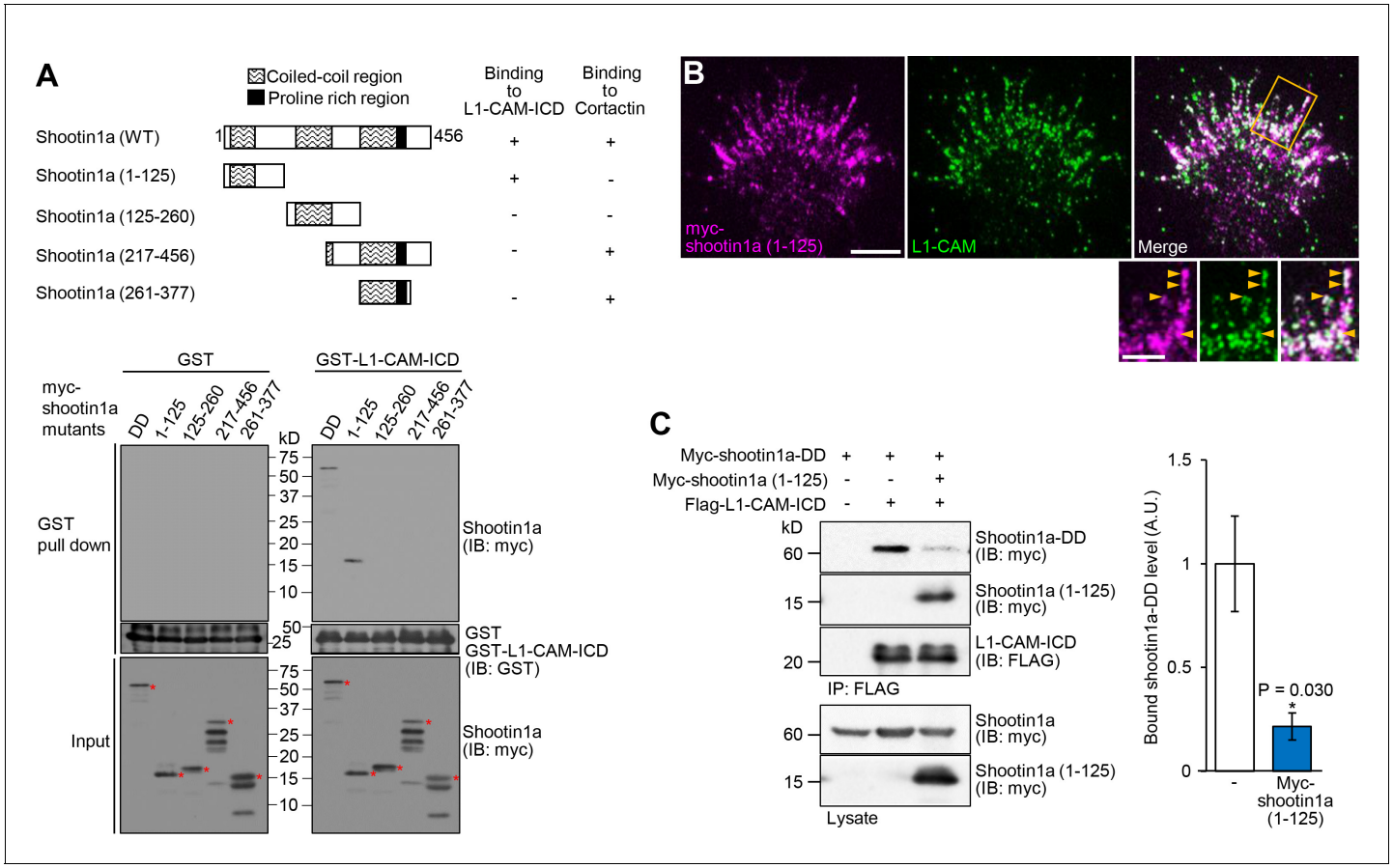

Figure 5. Shootin1a (1-125) interacts with L1-CAM and disturbs the interaction between shootin1a and L1-CAM. (**A**) Upper panel: schematic representation of shootin1a (WT) and shootin1a deletion mutants, and their ability to interact with L1-CAM-ICD and cortactin. Lower panel: in vitro binding assay using purified myc-tagged shootin1a mutants and purified GST-L1-CAM-ICD. Myc-shootin1a mutants (100 nM) were incubated with GST-L1-CAM-ICD (100 nM) and Glutathione Sepharose 4B. GST-L1-CAM-ICD was eluted. After SDS-PAGE, the eluate was immunoblotted with anti-myc or anti-GST antibody. Asterisks denote myc shootin1a mutants. (**B**) Neurons transfected with myc-shootin1a (1-125) were labeled with anti-myc (magenta) and anti-L1-CAM (green) antibodies. The cells were observed using a TIRF microscope. An enlarged view of the filopodium in the rectangle is shown in the inset. Arrowheads indicate shootin1a (1-125) colocalized with L1-CAM. Bar: 5 µm (in the inset, 2 µm). (**C**) Overexpressed shootin1a (1-125) inhibits the interaction between shootin1a and L1-CAM-ICD. HEK293T cells were transfected with vectors to express myc-shootin1a and FLAG-L1-CAM-ICD; some of them were also co-transfected with a vector to overexpress myc-shootin1a (1-125) as indicated. Cell lysates were prepared and incubated with anti-FLAG antibody. The immunoprecipitates were immunoblotted with anti-myc or anti-FLAG antibody. The cell lysates (1%) were also analyzed with anti-myc antibody. The graph (right) shows quantitative data for bound shootin1a-DD (n = 3 independent experiments). Data represent means ± SEM; *p<0.05 (unpaired Student's t-test).

DOI: https://doi.org/10.7554/eLife.34593.022

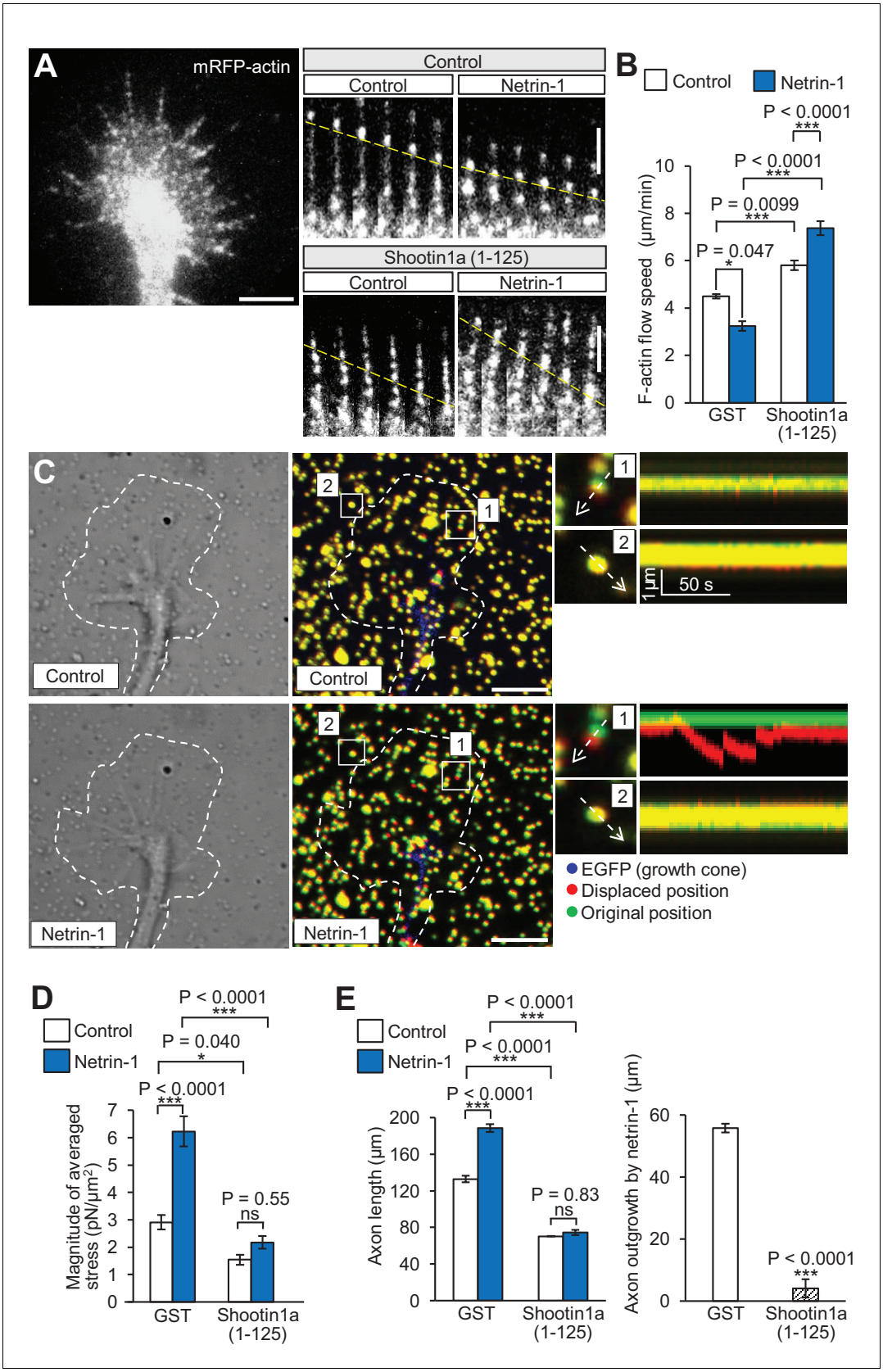

Figure 6. Shootin1a–L1-CAM interaction mediates netrin-1–induced F-actin adhesion coupling and mechanoresponse for axon outgrowth. (**A**) Fluorescent feature images of mRFP-actin at axonal growth cones overexpressing myc-GST (control) or myc-shootin1a (1-125) in the absence (control) or

Figure 6 continued on next page

Figure 6 continued

presence of 4.4 nM netrin-1 (see ***Video 2***). Kymographs of the fluorescent features of mRFP-actin in filopodia at 5 s intervals are shown (F-actin flows are indicated by dashed yellow lines). (**B**) F-actin retrograde flow speed measured from the kymograph analysis in A; 120 fluorescent features (47 growth cones) were analyzed. One-way ANOVA with Tukey's post hoc test was used. (**C**) DIC and fluorescence images (left panel) showing an axonal growth cone of a DIV2 neuron overexpressing EGFP and cultured on L1-CAM–coated polyacrylamide gel with embedded 200 nm fluorescent beads. The panels show representative images from time-lapse series taken every 3 s for 150 s before (control) and 60 min after netrin-1 (4.4 nM) stimulation (see ***Video 3***). The original and displaced positions of the beads in the gel are indicated by green and red colors, respectively. Dashed lines indicate the boundary of the growth cone. The kymographs (right panel) along the axis of bead displacement (white dashed arrows) at the indicated areas 1 and 2 of the growth cone show movement of beads recorded every 3 s. The bead in area two is a reference bead. (**D**) Analyses of the magnitude of the traction forces under axonal growth cones overexpressing myc-GST (control) or myc-shootin1a (1-125) before (control) or after netrin-1 stimulation (see ***Figure 6—figure supplement 1A*** for the direction of the traction forces, n = 14 growth cones). One-way ANOVA with Tukey's post hoc test was performed. (**E**) Three hours after plating, hippocampal neurons overexpressing myc-GST (control) or myc-shootin1a (1-125) were incubated with BSA (control) or 4.4 nM netrin-1 for 40 hr, and then immunolabeled by anti-myc antibody (see ***Figure 6—figure supplement 1B***). Axon length was then analyzed (n = 909 neurons). One-way ANOVA with Schaffer's post hoc test was performed in the left graph, while an unpaired Student's t-test was used in the right graph. Data represent means ± SEM; ***$p<0.01$; *$p<0.05$; ns, not significant. Bars: 5 μm (in the kymographs of A, 2 μm).

DOI: https://doi.org/10.7554/eLife.34593.024

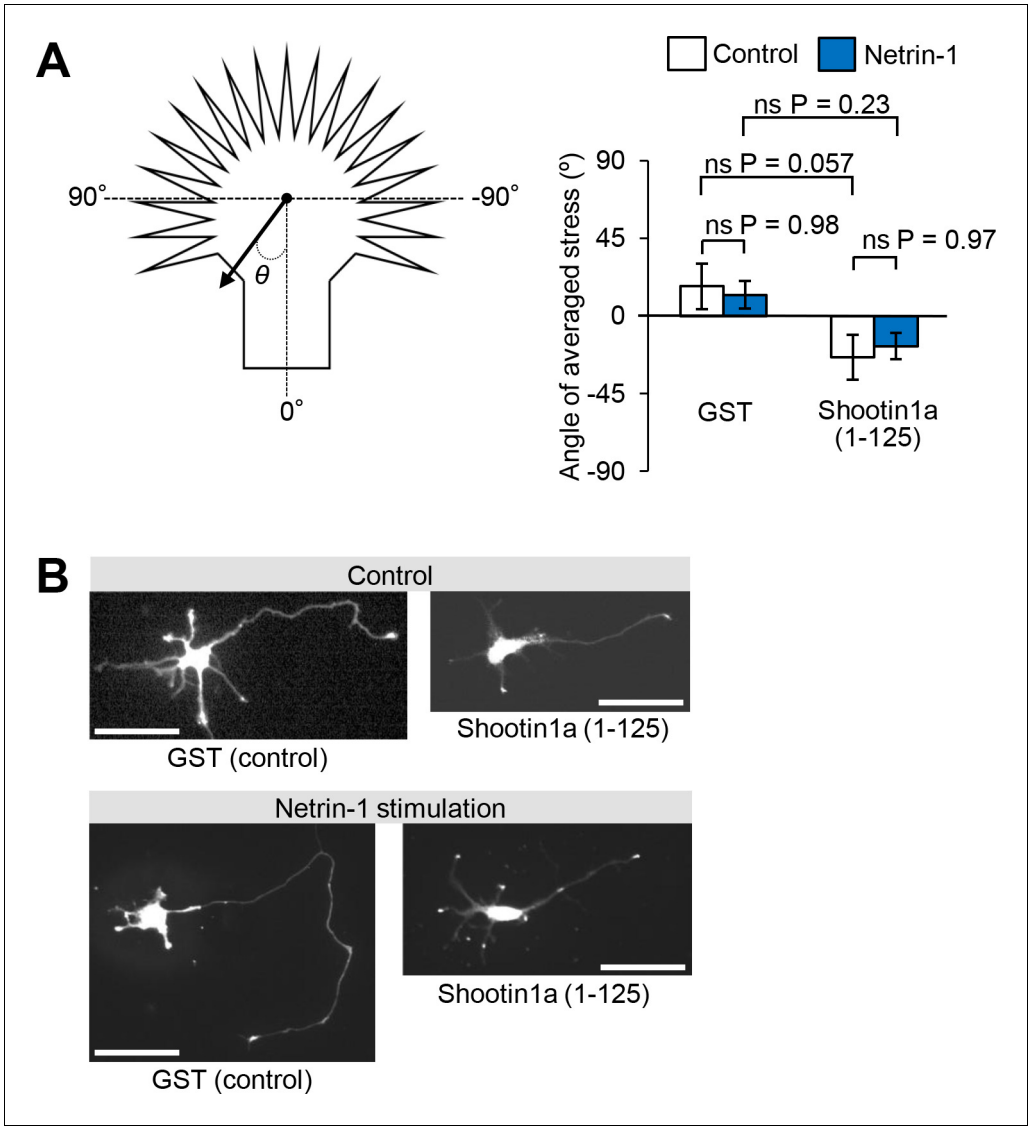

Figure 6—figure supplement 1. Shootin1a–L1-CAM interaction mediates netrin-1–induced axon outgrowth. (**A**) Statistical analyses of the angle (°) of the traction forces under axonal growth cones overexpressing myc-GST (control) or myc-shootin1a (1-125) before (control) or after netrin-1 stimulation (see ***Figure 6C and D***, n = 14 growth cones). Data represent means ± SEM; ns, not significant (one-way ANOVA with Tukey's post hoc test). (**B**) Three hours after plating, hippocampal neurons overexpressing myc-GST (control) or myc-shootin1a (1-125) were incubated with BSA (control) or 4.4 nM netrin-1 for 40 hr; they were then immunolabeled by anti-myc antibody (see also quantitative data in ***Figure 5E***). Bars: 50 μm.

DOI: https://doi.org/10.7554/eLife.34593.025

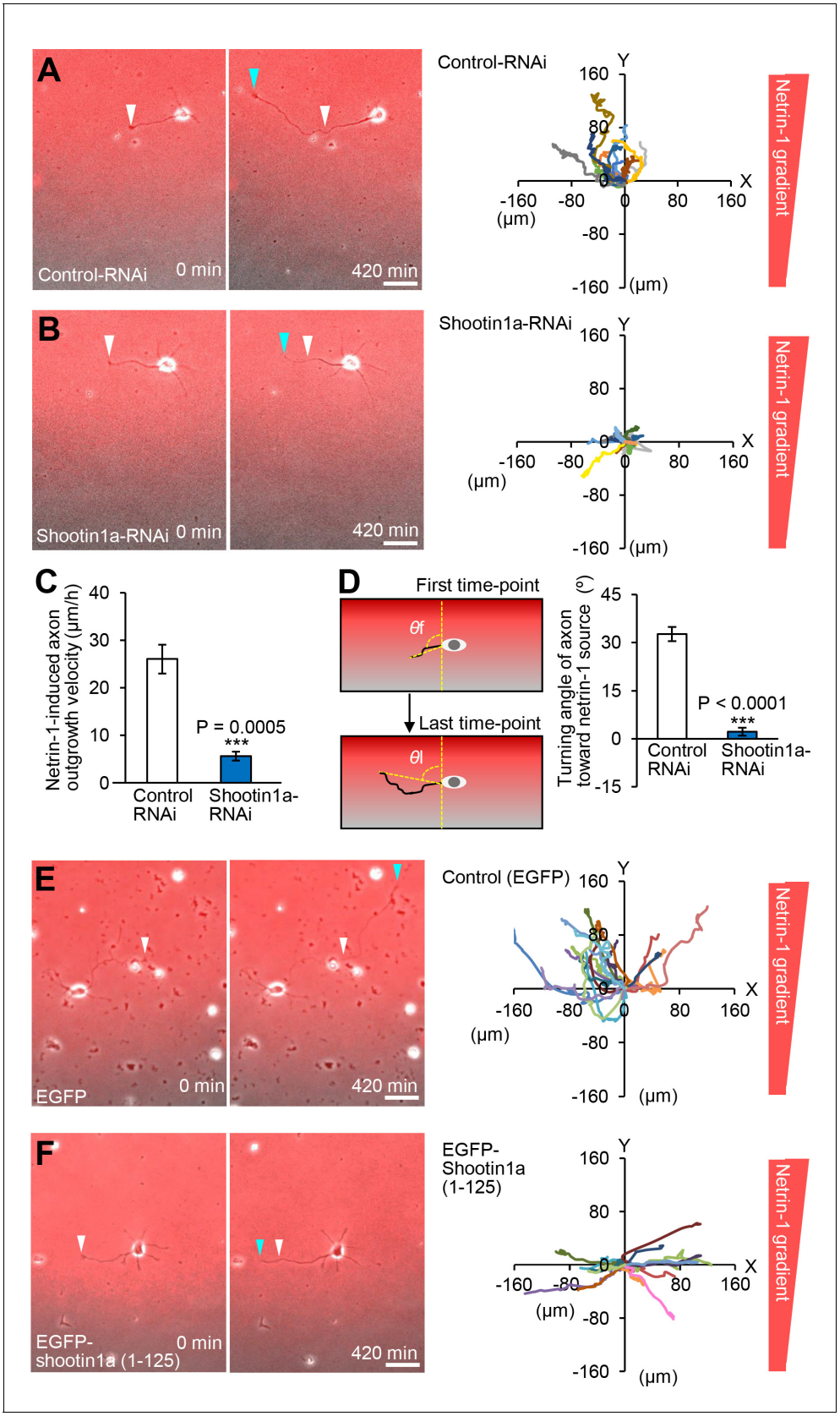

Figure 7. Shootin1a and shootin1a–L1-CAM interaction mediate netrin-1–induced axon guidance. (**A** and **B**) Time-lapse phase-contrast/fluorescence images of hippocampal neurons expressing control miRNA (**A**) and shootin1a miRNA (**B**) under the gradients of netrin-1 and Alexa Fluor 594-BSA.

Figure 7 continued on next page

Figure 7 continued

White and blue arrowheads indicate growth cones at the first and last time-points, respectively. See ***Videos 6*** and ***7***. The right panels depict trajectories of individual growth cone migrations. The initial growth cone positions are normalized at (x = 0 μm, y = 0 μm). Bars: 50 μm. (**C**) Axon outgrowth velocity obtained from the analyses in (**A** and **B**) (n = 24 growth cones). See also the legend for ***Figure 8C*** about quantitative data. (**D**) Turning angle of axon toward the netrin-1 source was obtained from the analyses in (**A** and **B**), by calculating the difference between the angles of the axonal tip at the first and last time-points of the observations (θf - θl). The graph shows quantified data (n = 24 growth cones). See also the legend for ***Figure 8D*** about quantitative data. (**E** and **F**) Time-lapse phase-contrast/fluorescence images of hippocampal neurons expressing EGFP (control) (**E**) and EGFP-shootin1a (1-125) (**F**) under gradients of netrin-1 and Alexa Fluor 594-BSA (red). White and blue arrowheads indicate growth cones at the first and last time-points, respectively. See ***Videos 8*** and ***9***. The right panels depict trajectories of individual growth cone migrations. The initial growth cone positions are normalized at (x = 0 μm, y = 0 μm). See also quantitative data in ***Figure 7—figure supplement 3***. Bars: 50 μm. Data represent means ± SEM; ***p<0.01 (one-way ANOVA with Schaffer's post hoc test).

DOI: https://doi.org/10.7554/eLife.34593.034

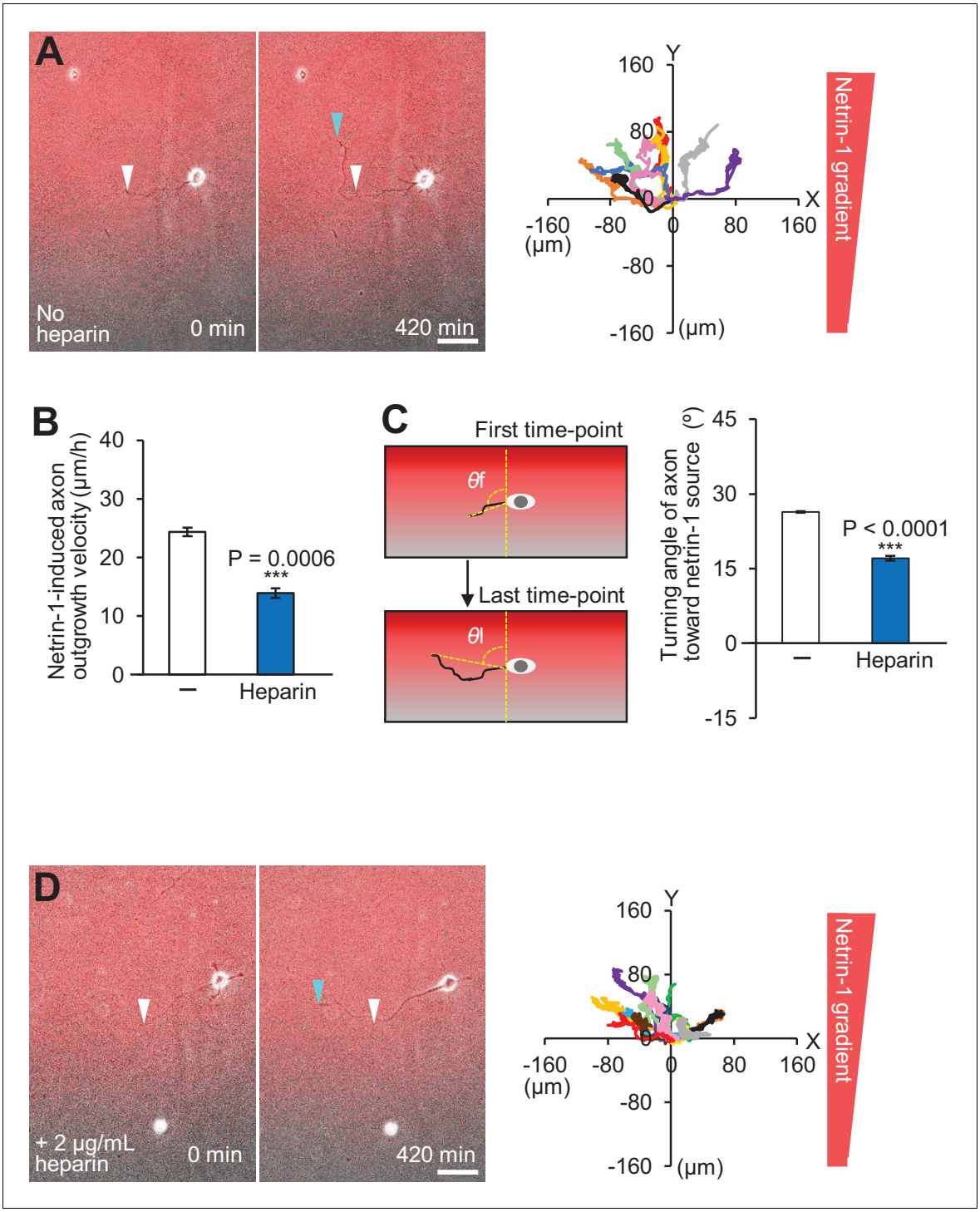

Figure 7—figure supplement 1. Soluble and substrate-bound netrin-1 contribute to axon turning. (**A** and **D**) Time-lapse phase-contrast/fluorescence images of hippocampal neurons under the gradients of netrin-1 and Alexa Fluor 594-BSA without (**A**) and with (**D**) 2 µg/ml heparin. White and blue arrowheads indicate growth cones at the first and last time-points, respectively. See ***Videos 4*** and ***5***. The right panels depict trajectories of individual growth cone migrations. The initial growth cone positions are normalized at (x = 0 µm, y = 0 µm). Bars: 50 µm. (**B**) Axon outgrowth velocity obtained from the analyses in (**A** and **D**) (n = 22 growth cones). (**C**) Turning angle of axon toward the netrin-1 source was obtained from the analyses in (**A** and **D**), by calculating the difference between the angles of the axonal tip at the first and last time-points of the observations (θf - θl). The graph shows quantified data (n = 22 growth cones). Data represent means ± SEM; ***p<0.01 (unpaired Student's t-test).

DOI: https://doi.org/10.7554/eLife.34593.035

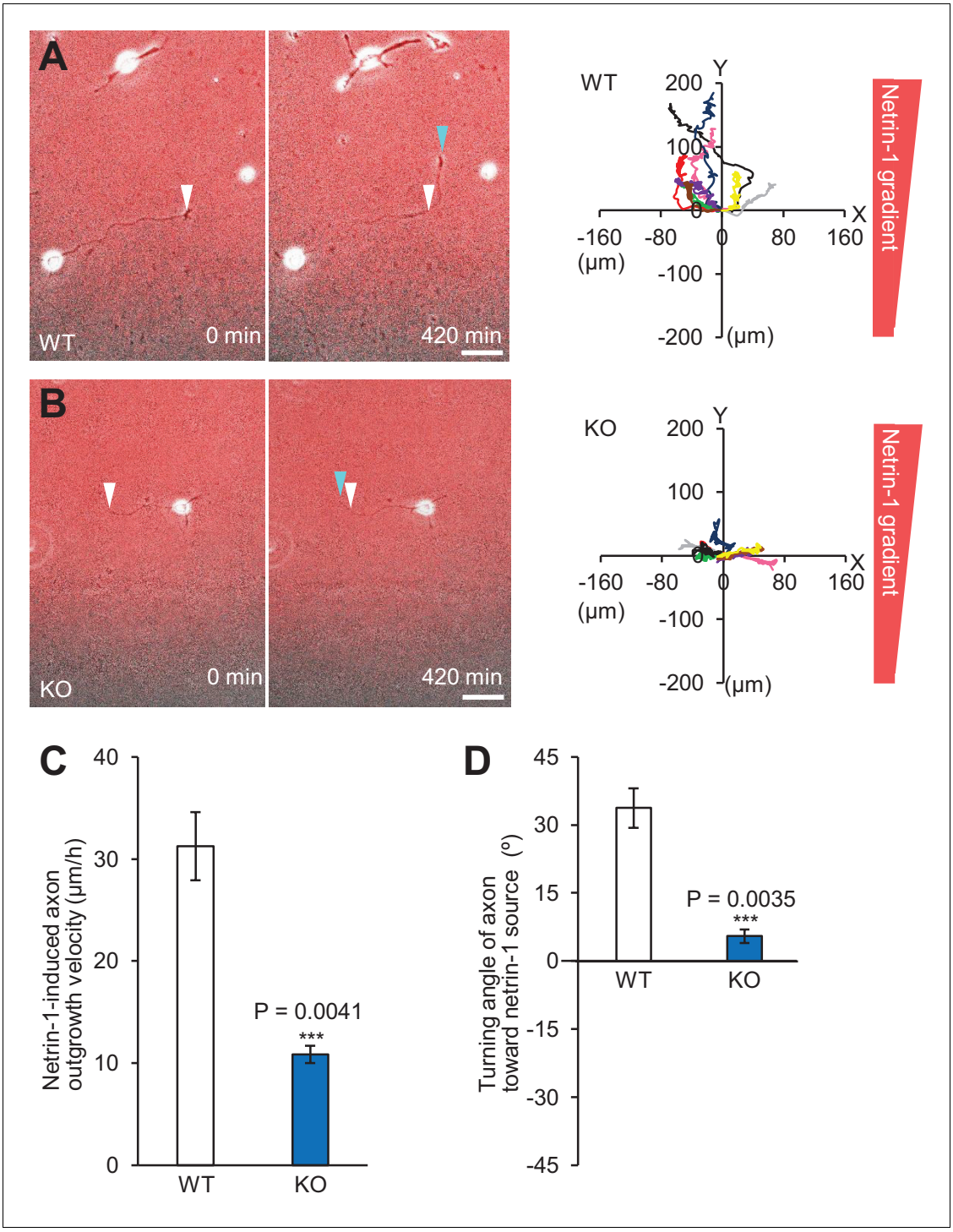

Figure 7—figure supplement 2. *Shootin1* knockout leads to inhibition of netrin-1–induced axon outgrowth and turning. (**A** and **B**) Time-lapse phase-contrast/fluorescence images of wild-type (**A**) and *Shootin1* knockout (**B**) neurons under the gradients of netrin-1 and Alexa Fluor 594-BSA. White and blue arrowheads indicate growth cones at the first and last time-points, respectively. The right panels depict trajectories of individual growth cone migrations. The initial growth cone positions are normalized at (x = 0 μm, y = 0 μm). Bars: 50 μm. (**C**) Axon outgrowth velocity obtained from the analyses in (**A** and **B**) (n = 18 growth cones). (**D**) Turning angle of axon toward the netrin-1 source was obtained from the analyses in (**A** and **B**), by calculating the difference between the angles of the axonal tip at the first and last time-points of the observations (θf - θl). The graph shows quantified data (n = 18 growth cones). Data represent means ± SEM; ***p<0.01 (unpaired Student's t-test).

DOI: https://doi.org/10.7554/eLife.34593.038

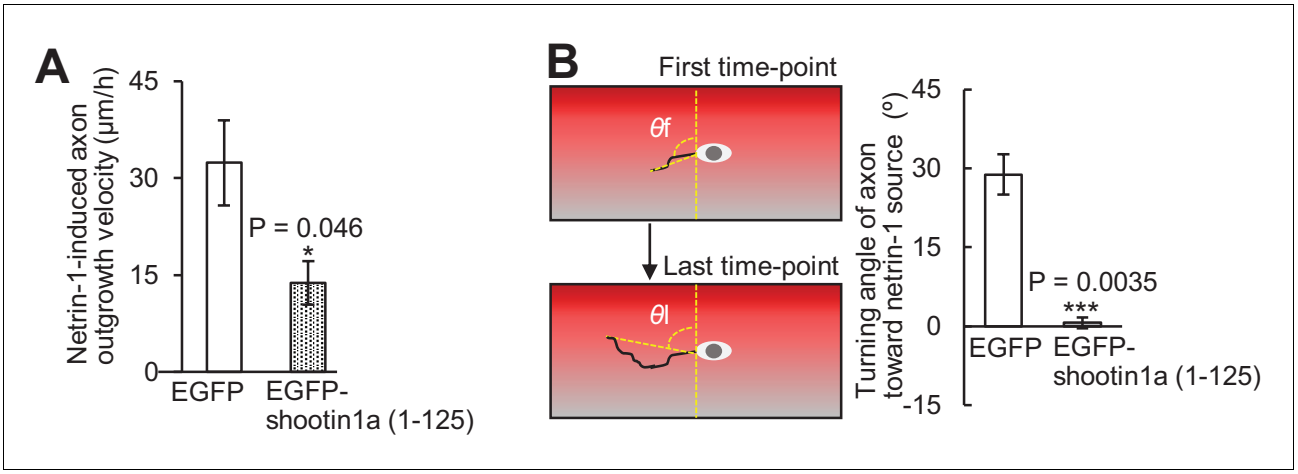

Figure 7—figure supplement 3. Shootin1a–L1-CAM interaction mediates netrin-1–induced axon guidance. (**A**) Axon outgrowth velocity obtained from the analyses in ***Figure 7E and F*** (n = 33 growth cones). (**B**) Turning angle of axon toward the netrin-1 source was obtained from the analyses in ***Figure 7E and F***, by calculating the difference between the angles of the axonal tip at the first and last time-points of the observations (θf - θl). The graph shows quantified data (n = 33 growth cones). Data represent means ±SEM; ***, $p<0.01$; *, $p<0.05$ (unpaired Student's t-test).

DOI: https://doi.org/10.7554/eLife.34593.041

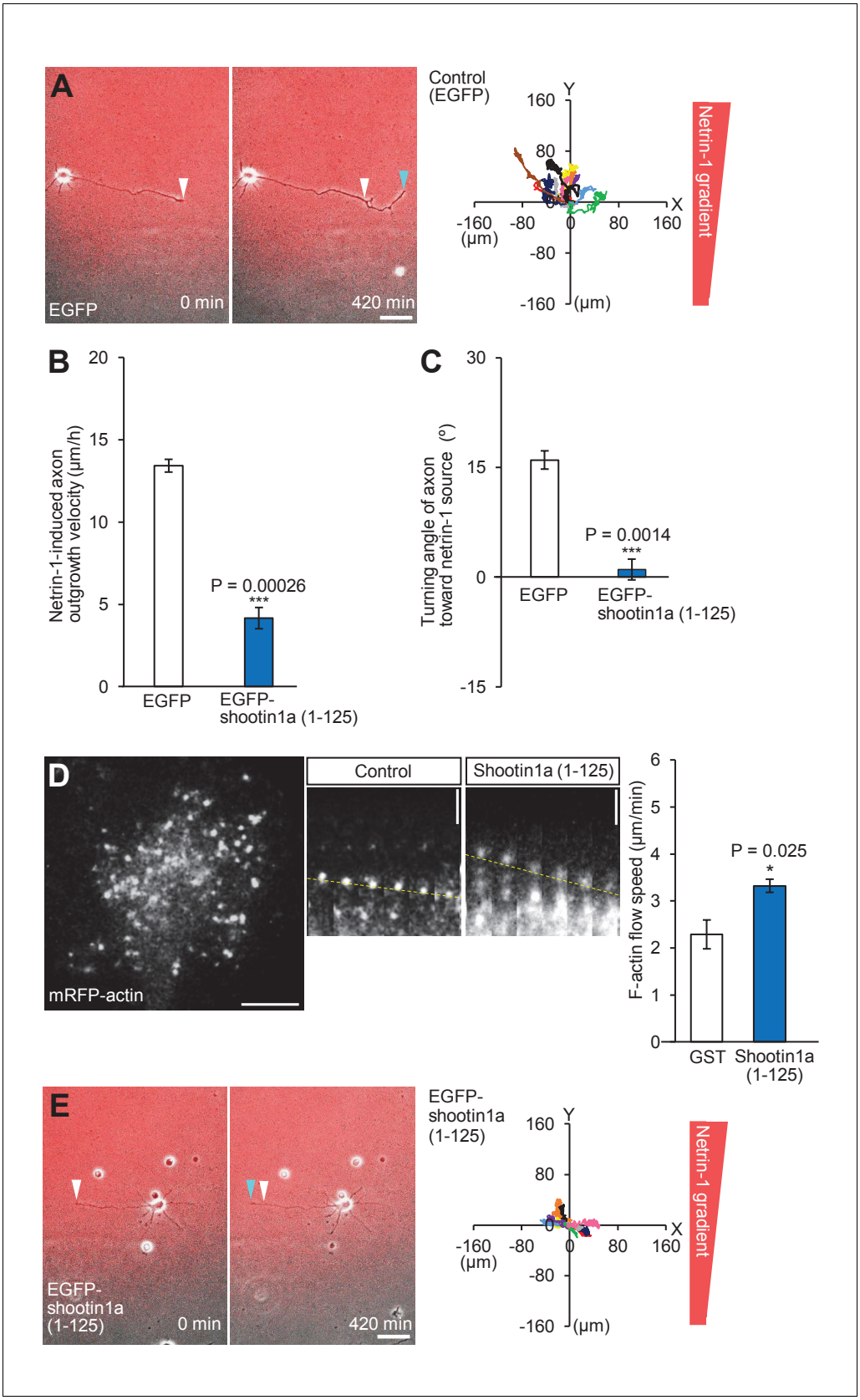

Figure 7—figure supplement 4. Shootin1a–L1-CAM interaction mediates netrin-1–induced axon guidance on laminin. (**A** and **E**) Time-lapse phase-contrast/fluorescence images of hippocampal neurons expressing EGFP (control) (**A**) and EGFP-shootin1a (1-125) (**E**) on a laminin surface under

Figure 7—figure supplement 4 continued on next page

Figure 7—figure supplement 4 continued

gradients of netrin-1 and Alexa Fluor 594-BSA (red). White and blue arrowheads indicate growth cones at the first and last time-points, respectively. The right panels depict trajectories of individual growth cone migrations. The initial growth cone positions are normalized at (x = 0 μm, y = 0 μm). Bars: 50 μm. (**B**) Axon outgrowth velocity obtained from the analyses in (**A** and **E**) (*n* = 21 growth cones). (**C**) Turning angle of axon toward the netrin-1 source was obtained from the analyses in (**A** and **E**), by calculating the difference between the angles of the axonal tip at the first and last time-points of the observations (θf - θl). The graph shows quantified data (*n* = 21 growth cones). (**D**) Fluorescent feature images of mRFP-actin at axonal growth cones overexpressing myc-GST (control) or myc-shootin1a (1-125) on a laminin surface. Kymographs of the fluorescent features of mRFP-actin in filopodia at 5 s intervals are shown (F-actin flows are indicated by dashed yellow lines). F-actin retrograde flow rate measured from the kymograph analysis; 50 fluorescent features (10 growth cones) were analyzed. Data represent means ± SEM; ***p<0.01; *p<0.05 (unpaired Student's *t*-test). Bar: 5 μm (in the kymographs, 2 μm).

DOI: https://doi.org/10.7554/eLife.34593.044

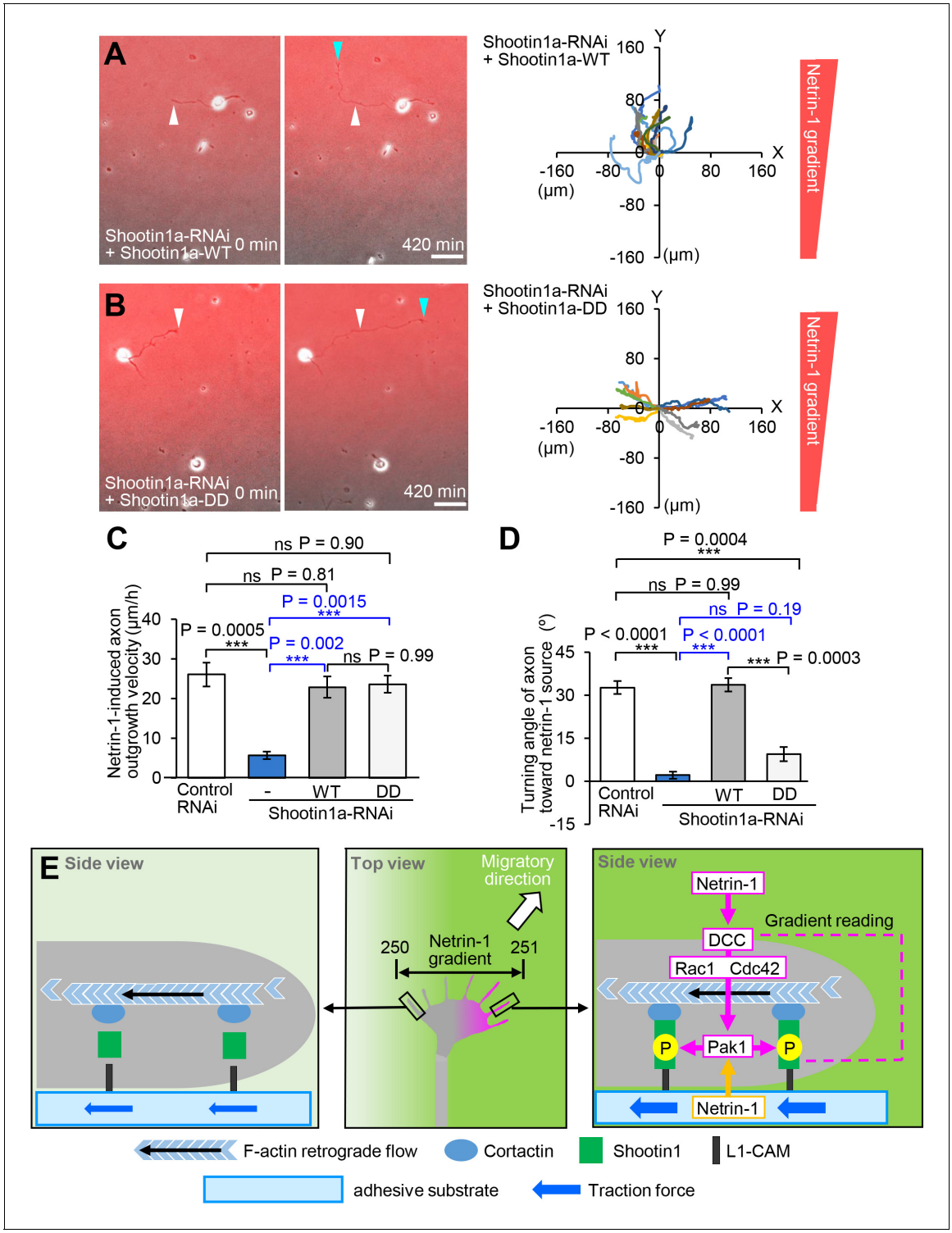

Figure 8. Asymmetric shootin1a phosphorylation within growth cones is required for netrin-1–induced axon guidance. (**A** and **B**) Time-lapse phase-contrast/fluorescence images of hippocampal neurons expressing shootin1a miRNA + RNAi refractory shootin1a-WT (**A**), and shootin1a miRNA + RNAi refractory shootin1a-DD (**B**) under gradients of netrin-1 and Alexa Fluor 594-BSA (red). White and blue arrowheads indicate growth cones at the first and last time-points, respectively. See ***Videos 10*** and ***11***. The right panels depict trajectories of individual growth cone migrations. The initial growth cone positions are normalized at (x = 0 µm, y = 0 µm). (**C**) Axon outgrowth velocity obtained from the analyses in ***Figure 7A and B***, ***Figure 8A and B*** (n = 47 growth cones). (**D**) Turning angle of axon toward the netrin-1 source was obtained from the analyses in ***Figure 7A and B***, ***Figure 8A and B*** (n = 47 growth cones), by calculating the difference between the angles of the axonal tip at the first and last time-points of the observations (θf - θi). (**E**)

Figure 8 continued on next page

Figure 8 continued

A model for gradient-reading and mechanoresponse processes of netrin1–induced axon guidance. A very small difference (250:251; 0.4%) in netrin-1 concentration can induce highly polarized phosphorylation of shootin1a within growth cones (pink), as a readout of highly sensitive gradient-reading processes. A netrin-1 gradient on the substrate would also contribute to polarized shootin1 phosphorylation (yellow). This process is achieved through a signaling pathway including DCC, Rac1/CDC42, Pak1 and shootin1a. The polarized phosphorylation of shootin1a within a growth cone locally promotes shootin1a–L1-CAM and shootin1a–cortactin interactions. These interactions in turn enhance asymmetrically the coupling between F-actin retrograde flow and the adhesive substrate and increase traction force (blue arrows) on the side of the netrin-1 source, thereby leading to a decision for the migratory direction (white arrow). Data represent means ± SEM; ***p<0.01; ns, not significant (one-way ANOVA with Schaffer's post hoc test). Bars: 50 μm.

DOI: https://doi.org/10.7554/eLife.34593.054